Stauffenberg, Jaqueline; Ortlepp, Ingo; Belkner, Johannes; Dontsov, Denis; Langlotz, Enrico; Hesse, Steffen; Rangelow, Ivo W.; Manske, Eberhard

Measurement precision of a planar nanopositioning machine with a range of motion of Ø100 mm

Original published in:	Applied Sciences. - Basel : MDPI. - 12 (2022), 15, p. 1-14.
Original published:	2022-08-04
ISSN:	2076-3417
DOI:	10.3390/app12157843
[*Visited:*	2022-09-16]

This work is licensed under a Creative Commons Attribution 4.0 International license. To view a copy of this license, visit https://creativecommons.org/licenses/by/4.0/

TU Ilmenau | Universitätsbibliothek | ilmedia, 2022
http://www.tu-ilmenau.de/ilmedia

Article

Measurement Precision of a Planar Nanopositioning Machine with a Range of Motion of Ø100 mm

Jaqueline Stauffenberg [1,*,†], Ingo Ortlepp [1], Johannes Belkner [1,†], Denis Dontsov [2], Enrico Langlotz [2], Steffen Hesse [3], Ivo Rangelow [4] and Eberhard Manske [1,*]

[1] Production and Precision Measurement Technology Group, Institute of Process Measurement and Sensor Technology, Technische Universität Ilmenau, Gustav-Kirchhoff-Straße 1, 98693 Ilmenau, Germany
[2] SIOS Meßtechnik GmbH, Am Vogelherd 46, 98693 Ilmenau, Germany
[3] IMMS Institut für Mikroelektronik- und Mechatronik-Systeme gemeinnützige GmbH (IMMS GmbH), Ehrenbergstraße 27, 98693 Ilmenau, Germany
[4] nano analytik GmbH, Ehrenbergstraße 1, 98693 Ilmenau, Germany
* Correspondence: jaqueline.stauffenberg@tu-ilmenau.de (J.S.); eberhard.manske@tu-ilmenau.de (E.M.)
† These authors contributed equally to this work.

Abstract: This work deals with various investigations into the accuracy of a newly developed planar nanopositioning machine. This machine, called Nanofabrication Machine 100 (NFM-100), has a positioning range of 100 mm in diameter. To determine the precision, various movement scenarios are performed with the machine table, and the trajectory deviation from the set trajectory is determined. In particular, the focus is on high velocities of up to 20 mm/s. Even at high speeds in the range of several millimetres per second, this machine can impress with its performance and only has a deviation in the nanometre range.

Keywords: nanopositioning machine; planar direct drive; sub-nanometre precision; macroscopic working range; high speed

Citation: Stauffenberg, J.; Ortlepp, I.; Belkner, J.; Dontsov, D.; Langlotz, E.; Hesse, S.; Rangelow, I.; Manske, E. Measurement Precision of a Planar Nanopositioning Machine with a Range of Motion of Ø100 mm. *Appl. Sci.* **2022**, *12*, 7843. https://doi.org/10.3390/app12157843

Academic Editors: Guanhao Wu, Xiuguo Chen and Yuki Shimizu

Received: 16 June 2022
Accepted: 2 August 2022
Published: 4 August 2022

Publisher's Note: MDPI stays neutral with regard to jurisdictional claims in published maps and institutional affiliations.

Copyright: © 2022 by the authors. Licensee MDPI, Basel, Switzerland. This article is an open access article distributed under the terms and conditions of the Creative Commons Attribution (CC BY) license (https://creativecommons.org/licenses/by/4.0/).

1. Introduction

In recent decades, new levels of complexity and miniaturisation have been reached in micro- and nanotechnology manufacturing [1]. As described in various road maps such as the ITRS or IRDS, structure sizes continue to decrease, while wafer sizes increase in order to achieve the highest possible throughput [2,3]. Highly accurate metrology is needed to achieve reproducible and error-free fabrication as well as the imaging of structures in various fields, such as nanoelectronics and semiconductors [4].

In the fabrication as well as the characterisation of nanostructures, many different alternative tools, in contrast to conventional methods, have been established, such as optical systems, tip-based systems as well as imprint tools [5]. However, most of these established technologies are limited to their measurement range. Especially with tip-based methods such as atomic force microscopy [6], there are usually a few square micrometres of area available in which the surface can be scanned with high precision.

In order to meet these challenges of high-precision positioning and, at the same time, the possibility of positioning on large areas in the millimetre range, nanopositioning and nanomeasuring machines can fill this gap. In the past decades, numerous research groups have worked on the development and improvement of nanopositioning technology [7].

For more than 20 years now, the Institute for Process Measurement and Sensor Technology at the Technische Universität Ilmenau has invested a great deal of work in the development of nanopositioning technology. The first three-dimensional positioning machine was developed with a movement range of 25 mm × 25 mm × 5 mm [8]. Subsequently, another machine was developed with a much larger measuring and movement range:

200 mm × 200 mm × 25 mm [9]. With these machines, the focus was primarily on a large movement range in all three spatial axes (*x*, *y* and *z* direction).

These machines can be equipped with various tools. For example, they can be used for characterisation by means of an autofocus sensor or an atomic force microscope (AFM) and for the production of structures via direct laser writing (DLW), nanoimprint lithography (NIL) and tip-based via field emission scanning probe lithography (FESPL) [5].

Especially for wafer-based technologies, it is of particular importance to have a stable *z* axis, which is why, in the development of a new type of nanopositioning machine, it was decided to limit the range of motion to two dimensions.

This planar machine in combination with a tip-based measuring system was designed and developed by SIOS GmbH in cooperation with the companies IMMS GmbH and nano analytik GmbH in Ilmenau [10].

With its range of motion of Ø100 mm, this newly developed nanopositioning machine is used to explore atomic force microscopy on large surfaces with ultimate precision.

In previous contributions, the enormous potential of the combination of a tip-based measurement system and the nanopositioning technique could yield first results. Line scans over millimetre ranges [11] as well as area scans [10] could be demonstrated, where the tip-based system realises the movement in the *z* direction and the machine table moves the sample in the *x* and *y* direction.

In this paper, the focus lies on the positioning accuracy of the machine table itself, how the deviation from the given trajectory increases with higher speed. First of all, after the presentation and classification of various positioning systems, the machine which is used and its structure are explained in more detail. Subsequently, the components available are described and the basic control scheme is explained. The analysis of the positioning accuracy starts with the investigation of the static state in closed-loop control. The deviation from the predefined trajectory is to be considered in different traversing scenarios, such as linear and circular movements up to the maximum velocity of 20 mm/s. Additionally, the tip-based system can provide information about the *z* noise. This is shown by AFM scans on SiC steps with hundreds of picometre height by comparing the scans with the machine table switched on and off. The main focus of this contribution is the metrological investigation of the planar nanopositioning machine.

2. State of the Art—Nanopositioning and Nanomeasuring Machines

In general, different approaches are used in nanopositioning and nanomeasuring technology. These include the sample-scanning mode, mixed-scanning mode and scanning probe mode [12]. In the sample-scanning mode, the measuring tool remains in a fixed position while the sample is moved by a machine table. In the scanning probe mode, the measuring tool is moved in all three spatial directions while the sample to be investigated is fixed.

In 1890, Ernst Abbe described an important principle of length measuring technology, where the measuring apparatus is to be arranged in such a way that the distance to be measured forms the straight-line continuation of the graduation, serving as a scale [13,14]. In this measuring arrangement, length measuring deviations, which are caused by systematic or accidental tilting, are reduced [14].

This Abbe comparator principle [13] was further developed into the extended three-dimensional Abbe comparator [15,16]. The nanopositioning machines developed at the Technische Universität Ilmenau are based on this principle, as this concept offers the possibility of using the high accuracy of the laser interferometer for 3D measurements. Because in the sample-scanning mode the probe as well as the measuring system are attached to a metrological frame, the Abbe comparator principle is fulfilled in all three measuring axes in which the length- and angle measuring systems do not have to be displaced. Based on this concept, the nanopositioning and measuring machine NMM-1 was developed, where three interferometric length measuring systems intersect in the touching point of the probe [17]. This way, the Abbe comparator concept is complied in all three

directions of motion. In order to avoid higher-order error influences due to angular tilt, additional angular sensors are mounted. These sensors are detecting the angular tilt, which is compensated for by the drive system.

Due to the overall concept of the machine, a resolution of 0.1 nm and a measurement uncertainty of 9 nm can be achieved in the measuring range of 25 mm × 25 mm × 5 mm [8].

After evaluating and testing the NMM-1, experience was gained and a new nanopositioning and measuring machine—the so-called NPMM-200—was developed, which is also based on the sample-scan mode and allows a significantly larger measuring range of 200 mm × 200 mm × 25 mm as well as an increase in performance in terms of position resolution [18]. Here, a three-dimensional measurement uncertainty of 30 nm was achieved [4].

The company *IBS Precision* developed a machine with a significantly larger measuring range: the nanocoordinate measuring machine ISARA 400 with a positioning range of 400 mm × 400 mm × 100 mm. However, the mixed-scanning mode is used here, where the machine table and the measuring tool are moved. The Abbe principle is also fulfilled here, due to the arrangement of the interferometric length measuring systems. The ISARA 400 achieves a measuring resolution of 1.6 nm and a measuring uncertainty of 100 nm [19].

The positioning machines presented have been specially developed to be able to move in all three measuring axes. Particular attention was placed on enabling a high movement range in the z direction. For very sensitive measuring tools such as tip-based systems, however, it is essential to have a particularly stable z axis during the movement of the sample stage.

For this reason, the nanofabrication machine (NFM-100) was developed to demonstrate and investigate the combination of tip-based technology and nanopositioning technology. This machine only moves in the x and y direction within a movement range of 100 mm in diameter. In principle, it follows the same principle, i.e., the sample-scanning mode, as the NMM-1 and the NPMM-200 but without allowing movement in the z direction.

3. Setup of the Planar Nanopositioning Machine

The newly developed planar nanofabrication machine has been specially designed for measurement and fabrication processes on wafer sizes of 4 inches.

Figure 1 shows a side view of the machine setup itself. As mentioned, a tip-based measuring system is installed as a measuring tool. This AFM system uses active microcantilevers and has a three-dimensional motion range of 10 µm × 10 µm × 5 µm due to the piezo scanning unit. These self-actuated and self-sensing microcantilevers are induced to oscillate by a thermomechanical actuator. This actuator consists of different layers with different coefficients of thermal expansion. The deflection readout of the cantilever is realised by a Wheatstone bridge. Scanning speeds of up to 50 µm/s have already been demonstrated with this tip-based system [20].

The whole setup is operated in a climate-controlled and vibration-isolated environment. The slider is guided aerostatically on three air bearings from NewWay [21]. The position is measured by differential interferometers (IFM) [22]. The length measuring systems as well as the actuators are arranged in a single plane and at an angle of 120 degrees between each other, as can be seen in Figure 2.

Aerostatic guide elements were chosen for the demanding nanometre-precise positioning because they provide a number of advantages, such as extremely low friction and low vibration during the movement [21]. These elements are mounted to the machine slider and hover on the planar granite base of the NFM-100 (see Figure 3), supplied with pressurised air by flexible tubing. Because there is no mechanical contact with this type of guidance, stick–slip effects can be eliminated. In addition, these air bearings are characterised by high repeatability [23].

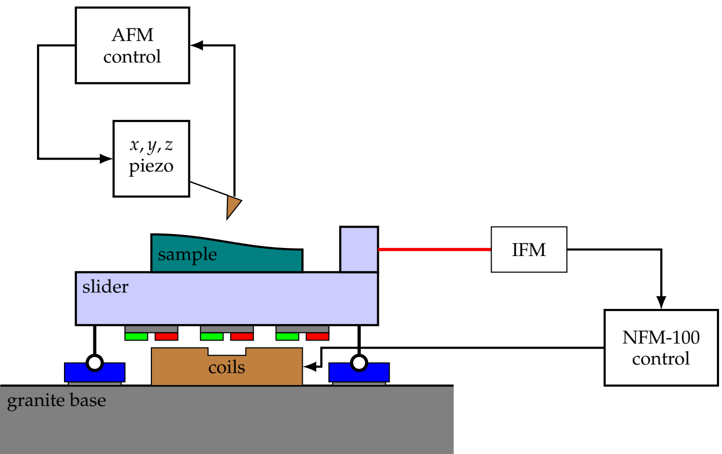

Figure 1. Side view of working principle of the planar nanopositioning machine and the installed tip-based system.

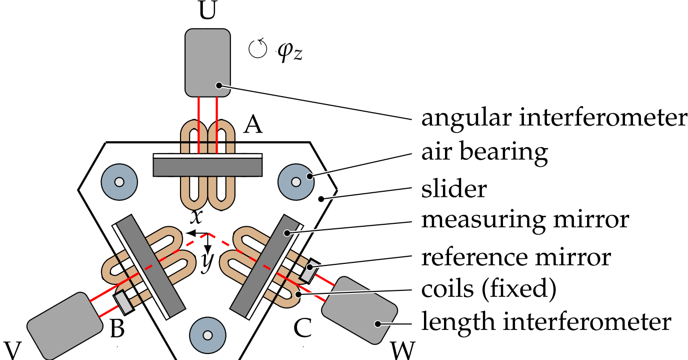

Figure 2. Mechanical and interferometer set-up of the NFM-100. The position of the slider is tracked by three laser-interferometers in a 120° arrangement. The slider is driven by three linear actuators, which consist of two flat coils and a magnet array each (magnet array not shown here). (Figure leaned on [11]).

For positioning of the slider, the NFM-100 uses a planar direct drive system. Three actuators based on electromagnetic force generation are used here, which enable a contactless force transfer. Each actuator consists of two fixed coils that act on magnets attached to the slider, i.e., the machine table. The drive forces of the three linear actuators act simultaneously on the slider. The 120° arrangement allows a resulting force in any direction within the x-y plane and additionally a rotation around the z axis can be generated [24]. Accordingly, this results in a circular range of motion.

Three differential plane-mirror interferometers, which offer especially high thermal stability due to their symmetric optical design, are used as length measurement systems [22]. The laser source for these differential interferometers is a stabilised He-Ne laser, which provides a relative frequency stability of 2×10^{-8}. The evaluation electronic uses an arctan demodulation technique with a path resolution of 5 pm [25].

By setting up the interferometers with an external reference beam, the measurement systems can be placed at a greater distance from the measurement location without significantly affecting the stability of the measurement [22]. In contrast, disturbances along the direction of measurement can be partially compensated by the differential design and, thus, noise in the length signal caused by air turbulence or vibrations can be cancelled out to a large extent.

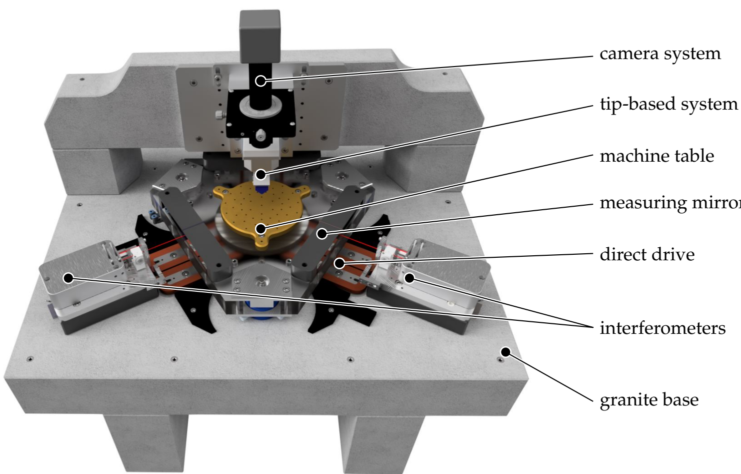

Figure 3. CAD model of the Nanofabrication Machine (NFM-100). The AFM measuring system is mounted directly above the centre of the machine table.

In the NFM-100, two interferometers are used for length measurement, while the third interferometer is used for angular measurement.

The two interferometers for length measurement are arranged in such a way that their measuring axes virtually intersect at the probing point of the measuring tool, so that the Abbe principle can be fulfilled in the x, y and z direction with an Abbe-offset $l_{Abbe,i} = 0$ [17] and an uncertainty $u_{Abbe,i} < 100\,\mu m$:

$$l_{Abbe,i} = 0 \pm u_{Abbe,i} \qquad i \in x, y, z \tag{1}$$

This way, first-order rotation-induced length measuring errors can be reduced to a minimum. Otherwise, the tilt φ of the slider around the x, y or z axis would lead to an Abbe-error Δl [17]:

$$\Delta l_{i,j} = u_{Abbe,i} \cdot sin(\varphi_j) \approx 0 \qquad i, j \in x, y, z. \tag{2}$$

The third interferometer, which is used for angle measurement, is arranged in such a way that the reference beam and the measuring beam both hit the moving mirror mounted on the machine slider. Based on the known spacing and the length difference of both interferometer beams, the rotation of the machine table around the z axis can be measured and compensated for by the control system. This is especially necessary as the mechanical design of the NFM-100 does not constrain this rotation. Therefore, the rotation must be actively measured and controlled to zero. The maximum rotation allowed here is 30′′. Because the rotor has no mechanical rotation lock, closed-loop operation is necessary. A dSpace© system is used here as the control system.

The following table (Table 1) shows the technical specifications of the nanofabrication machine presented here [26].

Table 1. Parameters of the positioning machine NFM-100.

Positioning range	Ø100 mm
Maximum velocity	$20\,\frac{mm}{s}$
Maximum acceleration	$250\,\frac{mm}{s^2}$
Interferometer resolution	5 pm
Maximum added mass	2 kg

In Figure 4, the basic structure of the control system is depicted. The measured variables are the three length values of the laser interferometers (U, V, W). These are transformed to the positioning coordinates (x, y, φ_z). The rotation of the stage around

the z-axis φ_z is calculated from towards the Abbe point symmetrically arranged probe beams of the U interferometer. φ_z is derived from this separation per angular displacement $\Delta l \approx 14\,\text{mm}/\text{rad}$. The angular displacement $\Delta_\varphi \leq 50\,\text{arcsec}$ are kept very small which allows for linearisations of trigonometric functions. Furthermore, the apparent cosine error originating from the distance between origin and U-mirror (compare Figure 2) becomes negligible. The implemented simplified reconstruction of the x- and y-axis from the measured length values states as:

$$T_{VWUxy\varphi} = \begin{pmatrix} -\frac{\sin(\alpha_W)}{\sin(\alpha_V-\alpha_W)} & \frac{\sin(\alpha_V)}{\sin(\alpha_V-\alpha_W)} & 0 \\ \frac{\cos(\alpha_W)}{\sin(\alpha_V-\alpha_W)} & -\frac{\cos(\alpha_V)}{\sin(\alpha_V-\alpha_W)} & 0 \\ 0 & 0 & \frac{1}{\Delta l} \end{pmatrix} \tag{3}$$

where $\alpha_W = -30^\circ$ and $\alpha_V = -150^\circ$ are the rotation angles of the V and W axis starting from x axis.

The core of the control system is formed by three separate classic PID controllers for each of these coordinates [24]. For $(x, y, \varphi_z)^T$, an independent PID controller in its standard form is employed:

$$\vec{a}(t) = K_P \odot \vec{e}(t) + K_I \odot \int_0^t \vec{e}(\tau)d\tau + K_D \odot \frac{d\vec{e}(t)}{dt} \tag{4}$$

where $\odot$ denotes the (element-wise) Hadamard product. Following the notation of Figure 4, the control error $\vec{e}$ is thereby given as:

$$\vec{e} = \begin{pmatrix} x \\ y \\ \varphi_z \end{pmatrix}_{set} - \begin{pmatrix} x \\ y \\ \varphi_z \end{pmatrix}_{real} \tag{5}$$

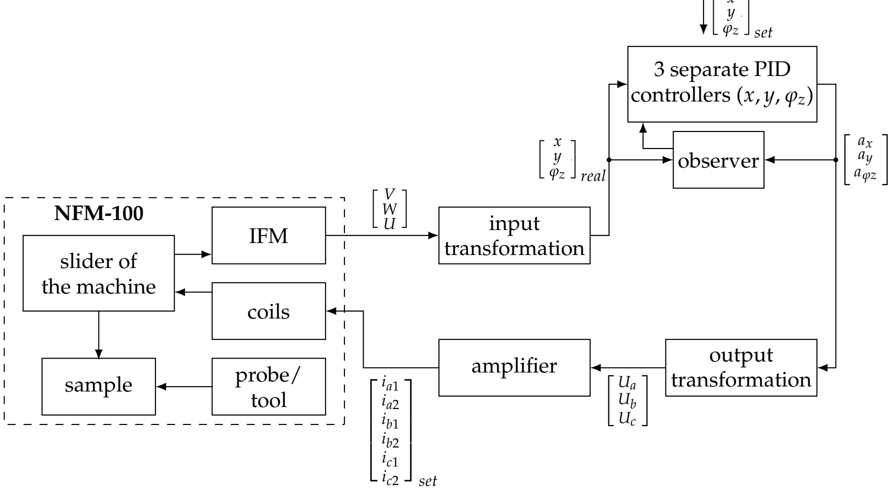

Figure 4. Control scheme of the NFM-100 and its positioning system.

The left side of Figure 5 shows the reconstructed transfer characteristics of the electromechanical system (plant), including the transformations. There are no significant disturbances in the relevant frequency range up to 50 Hz. The system then can be reduced to a double integrator and small damping term for all movement directions:

$$\begin{aligned} \frac{d\vec{x}}{dt} &= \begin{pmatrix} 0 & 1 \\ 0 & -\frac{d}{m} \end{pmatrix}\vec{x} + \begin{pmatrix} 0 \\ \frac{k_m}{m} \end{pmatrix} i \\ y &= \begin{pmatrix} 1 & 0 \end{pmatrix}\vec{x} \end{aligned} \tag{6}$$

where $\vec{x} = (x_1, x_2)^T$ and $y = x_1$ are the state-space variables for each movement direction $(x, y, \varphi_z)^T$. Assuming the mass of the platform $m = 9\,\mathrm{kg}$ as a well-defined value, the other plant parameters have been found as $d = 2.43\,\mathrm{kg/s}$ for the low-frequency damping constant and $k_m = 2.196\,\mathrm{N/A}$ the motor constant. The latter is in well agreement with electromagnetic simulation data, expecting $k_m = 2.24\,\mathrm{N/A}$. The rotational parameters for the φ_z-system can be derived in analogue manner using torques instead of forces.

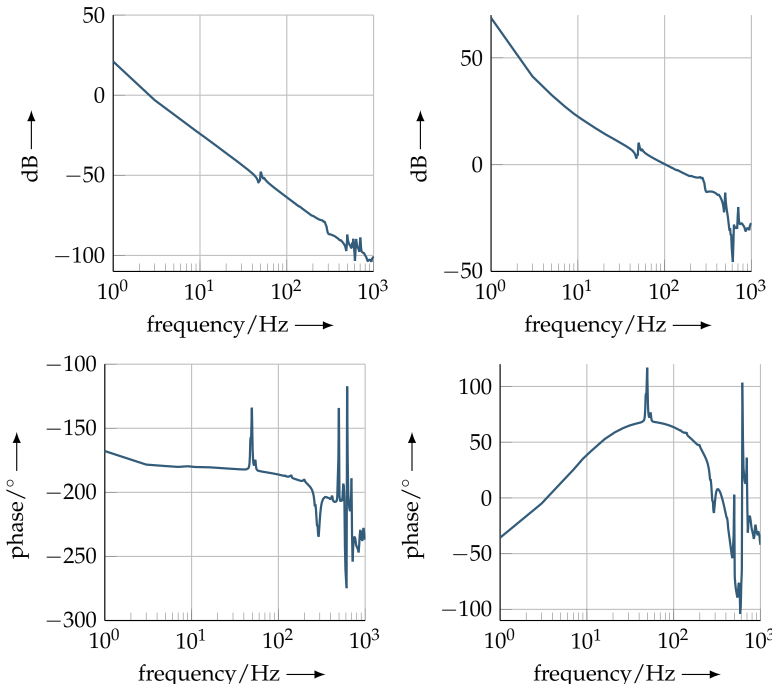

Figure 5. Comparison of the reconstructed transfer function of the plant alone (diagrams in the left half) and the open loop, including the controller (diagrams in the right half). The diagrams show the amplitude responses in decibels in the upper row and the phase responses in the lower row.

The PID controller has been designed within the pole-zero plane using the Nyquist stability criterion for each axis individually. The designed gains for Equation (4) are:

$$K_P = \begin{pmatrix} 400\times10^3\,\mathrm{s}^{-2} \\ 400\times10^3\,\mathrm{s}^{-2} \\ 50\times10^3\,\mathrm{s}^{-2} \end{pmatrix} \quad K_I = \begin{pmatrix} 3.0\times10^6\,\mathrm{s}^{-3} \\ 3.0\times10^6\,\mathrm{s}^{-3} \\ 400\times10^3\,\mathrm{s}^{-3} \end{pmatrix} \quad K_D = \begin{pmatrix} 500\,\mathrm{s}^{-1} \\ 500\,\mathrm{s}^{-1} \\ 900\,\mathrm{s}^{-1} \end{pmatrix} \tag{7}$$

It shall be noted that the integrator has been bounded to limit wind-up. The right side of Figure 5 shows the resulting open-loop response of the combined controller and plant. At the bandwidth limit at 100 Hz, a phase margin of comfortable 63° is kept to attain robustness. This is of particular importance, because specimens of different size and weight are frequently changed for examination.

At higher frequencies around $f > 500\,\mathrm{Hz}$, the plant shows several higher-order resonances of unidentified origin (left side of Figure 5). To prevent a sensitive reaction of the plant excited by PID controllers at these frequencies, the controller output is supressed through a notch filter from $f_1^N = 495\,\mathrm{Hz}$ to $f_2^N = 595\,\mathrm{Hz}$.

Besides its use for the PID design, the model is used to improve the state estimation through an observer. A steady-state Kalman filter will be employed for this purpose. The discrete state-space update equation for the Kalman filter is given for an individual moving direction as [27]:

$$\hat{\vec{x}}(n+1, n) = A_z(I - MC_z)\hat{\vec{x}}(n, n-1) + [B_z \quad A_zM][a_i(n), y_i(n)]^T \tag{8}$$

where $\hat{\vec{x}}$ are the estimates of the states from the measured and transformed noisy movement positions y_i and the PID controller output acceleration a_i. The noise co-variances are estimated to be $Q = 1$ for the plant and $R = 1\times10^{-10}$ for the measurement. With these follows an innovation of $M = (0.5027, 1721)^T$ and the specific Kalman filter as:

$$\hat{\vec{x}}(n+1,n) = \begin{pmatrix} 0.3253 & 0.0001 \\ -1721 & 1 \end{pmatrix} \hat{\vec{x}}(n,n-1) + \begin{pmatrix} 1.22\times10^{-6} & 0.6747 \\ 0.0244 & 1721 \end{pmatrix} \begin{pmatrix} a_i(n) \\ y_i(n) \end{pmatrix} \quad (9)$$

The used interferometers have a sub-nanometre measurement precision. Therefore, only the velocities $\vec{v} = (v_x, v_y, v_\varphi)^T$ shall be estimated by the filter. The lower row for $\hat{x}_2 = v_i$ of this Kalman filter provides this estimation. The velocity of the error therefore follows from Equation (5) as:

$$\frac{d\vec{e}(t)}{dt} \approx \begin{pmatrix} v_x \\ v_y \\ v_\varphi \end{pmatrix}_{set} - \begin{pmatrix} v_x \\ v_y \\ v_\varphi \end{pmatrix}_{est} \quad (10)$$

The resulting accelerations from (4), $\vec{a} = (a_x, a_y, a_\varphi)^T$, are scaled to currents via their respective motor constants and transformed to the three actuator axes. This actuation transformation differs from the measurement transformation given their different physical domain. For the three drives $(A, B, C)^T$, the transformation follows from the 120° arrangement and the force directions of the coils (compare Figure 2) as:

$$T_{xy\varphi ABC} = \begin{pmatrix} \frac{2}{3} & 0 & \frac{1}{3} \\ -\frac{1}{3} & \sqrt{\frac{1}{3}} & \frac{1}{3} \\ -\frac{1}{3} & -\sqrt{\frac{1}{3}} & \frac{1}{3} \end{pmatrix} \quad (11)$$

These currents $(i_A, i_B, i_C)^T$ are then split onto the two coils depending on their current position-dependent commutation. Magnetic fields of coils and magnets for this commutation are implemented via numerically simulated data.

In the following section, the deviation from the specified trajectory up to the maximum velocity of 20 mm/s is examined after considering the static condition for various movement scenarios.

4. Investigations and Measurement Results

In previous publications, the great potential of the NFM-100 in combination with a tip-based system was shown and statements were made about the accuracy [5,10,11,17]. In the following part, first, only the machine itself is considered in static operation and, subsequently, its performance at high movement speeds. Furthermore, the deviation from the specified trajectory is analysed for both linear and circular motion.

In the presented setup of the machine, there is no constraint for the x and y direction. Thus, a rotation around the z axis is allowed in principle. Through the use of air bearings, a higher linearity of the x and y movements can be achieved through almost friction- and force-free movement. This is further supported in terms of control technology through precise, permanent measurement and dynamic control of the rotation around the z axis by means of the three voice coil actuators.

Therefore, the position noise of the machine table with a sampling frequency of 10 kHz for a duration of 10 s in the x and y direction as well as the noise of the angle interferometer is first considered. In Figure 6, the recorded position noise in closed-loop control at the origin is depicted.

The standard deviation (1σ) of the different values are shown in the following table.

As can be seen in Table 2, the values fulfil the requirement of an extremely low positioning noise (<1 nm), which is necessary for precise AFM measurements. Moreover,

this is especially important for the fabrication of nanostructures, because they cannot be corrected afterwards.

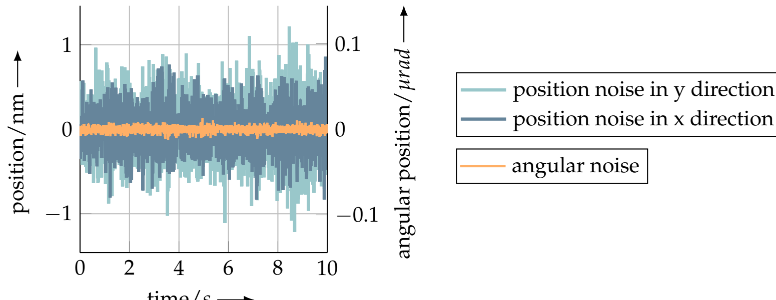

Figure 6. Positioning noise of the NFM-100 of the x and y interferometer (left y axis) as well as of the angle interferometer (right y axis) in closed-loop control for a duration of 10 s at the origin (0,0).

Table 2. Different values of positioning noise (1σ) in closed-loop control of the NFM-100 for a duration of 10 s and a sampling frequency of 10 kHz (see Figure 6).

Position noise in x direction	246 pm
Position noise in y direction	317 pm
Angular noise	3.4855 nrad

For the further investigation of the static operation, the machine table was moved to several points on the x and y axis, where the position noise was recorded. Figure 7 shows the points where the position noise was recorded within the entire range of motion.

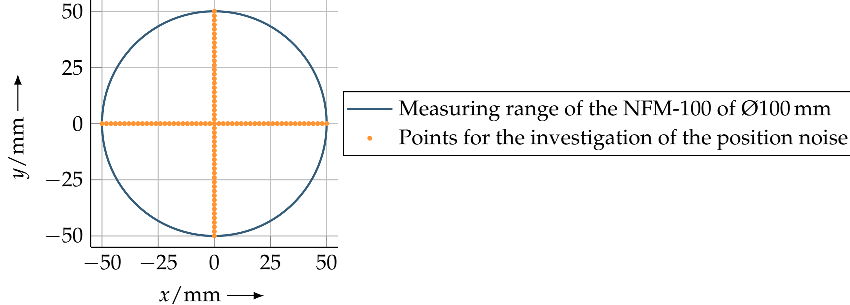

Figure 7. Investigated points for positioning noise over a range of 100 mm in x and y direction with a distance of 2 mm.

Initially, Figure 8 shows how the position stability behaves over the movement range of 100 mm in both the x and y direction. For this purpose, the position noise was recorded over a period of 10 s with a sampling frequency of 10 kHz, each at a distance of 2 mm on the x and y axis over a maximum distance of 100 mm (see Figure 7). For this purpose, the deviations of the x and y axis are plotted in each case.

Over the entire examined range, the maximum deviation is below 450 pm (1σ), as can be seen in Figure 8.

After this static investigation, the focus was placed on the dynamic mode.

First, straight-line trajectories were driven at different velocities. For this purpose, this analysis was carried out along the x axis as well as the y axis over a length of 50 mm and 100 mm. In this case, a velocity range between 0.5 mm/s and 20 mm/s was selected and investigated. Figure 9 shows that at the maximum velocity of 20 mm/s over a length of 100 mm, the maximum path deviation perpendicular to the moving direction is below 7 nm (6.545 nm).

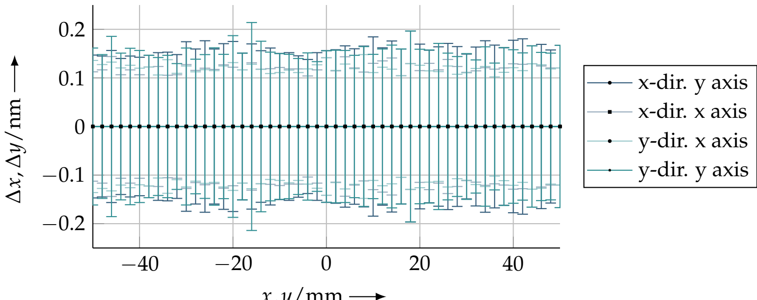

Figure 8. Positioning noise (1σ) of the x and y interferometer in x and y direction from position –50 mm to 50 mm in a distance of 2 mm. This noise was recorded for a time of 10 s each with a frequency of 10 kHz.

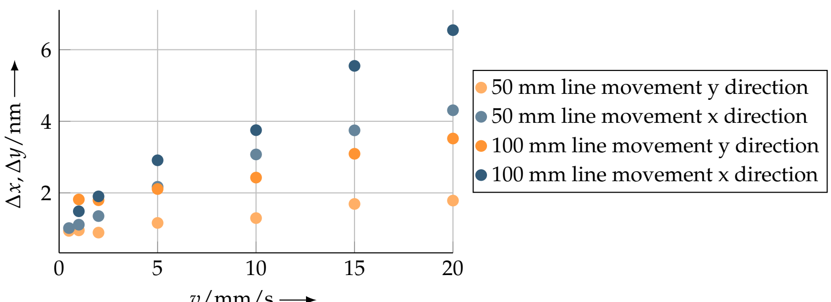

Figure 9. Straightness deviation for movements in x and y direction with a length of 50 mm and 100 mm. The dependence of the deviation of the line movement was investigated in a velocity range between 0.5 mm/s and the maximum velocity of 20 mm/s.

In addition, it can be seen that the movements in the y direction have a smaller deviation than in the x direction at the same velocity. This can be explained by the fact that when moving in the y direction, two actuators are used equally due to the symmetry of the actuator arrangement. Furthermore, the angular deviation during a line movement with a length of 100 mm at the maximum speed was considered. During line travel in the x direction, an angle deviation (1σ) of 714 nrad was measured. In the y direction, this measured deviation is 842 nrad.

In Figure 10, five consecutive revolutions with a nominal trajectory with a radius of 1 mm are shown. The movements were carried out at a circumferential velocity of 10 mm/s. In order to illustrate the deviations of the circular path more clearly, the original measurement data were transformed into polar coordinates, which is depicted in the following Figure 11.

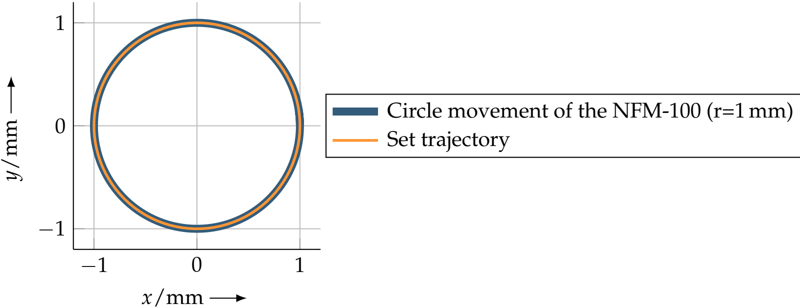

Figure 10. Positioning accuracy of a circle movement by the NFM-100 with a radius of 1 mm and a circumferential velocity of 10 mm/s. Here, the standard deviation of the radius is 3.107 nm (1σ). The angular φ_Z deviation in this case is 354 nrad.

In addition to this investigation, Figure 12 shows the path deviations of a circular movement as a function of velocity. Different radii were driven with the machine table at various velocities. The examined velocity range was between 0.1 mm/s and 20 mm/s. In this examination, circles with radii between 1 mm and 40 mm were driven at different speeds with five repetitions each. Also in this case, the standard deviation for the radius at the maximum velocity of 20 mm/s at r = 40 mm is 7.269 nm.

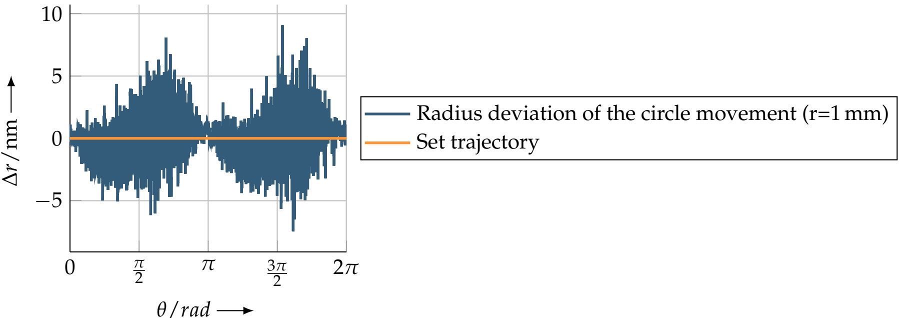

Figure 11. Radius deviation of a circle movement with 1 revolution ($\theta = 2\pi$, unwinding of circle in Figure 10).

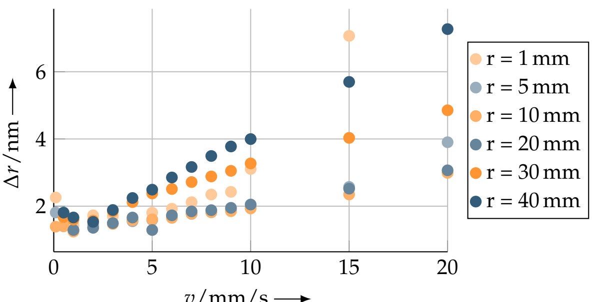

Figure 12. Deviation of circle movement of a given circle trajectory with radii between 1 mm and 40 mm at different velocities (0.1 mm/s–20 mm/s). The circular movement was carried out with 5 revolutions in each case.

For a circular movement with a diameter of 80 mm and a velocity of 20 mm/s, the maximum angular deviation is only 689 nrad.

As mentioned in Section 3, the selected air bearings are characterised by numerous advantages. However, a residual noise in the z direction is still present. To investigate this, the existing atomic force microscope (AFM) was used. An AFM scan was made on an area of 10 µm × 10 µm on a sample when the machine table was switched off and, thus, the machine table was directly resting on the granite machine base without an air layer in between. For comparison, a scan was measured when the table was switched on. For this purpose, a sample with a surface that has only very small steps (<1 nm) in the z direction was selected. Here, a SiC sample was used that has step heights of about 750 pm and step widths between 150 nm and 400 nm. The step height is equal to half of the lattice constant of the 6H-SiC crystal in the [0001] direction [28]. As shown in Figure 8, the position noise in the x and y direction is below 300 pm, which can be neglected for the AFM scan in that case.

Figure 13 (left and right) shows a topography scan of the aforementioned SiC sample with the difference between the machine table being switched off and on. The scanning speed for both measurements was 5 µm/s.

The individual steps are clearly visible in both pictures. However, in the picture with the machine table switched on, it can be seen that the amount of noise increases slightly.

In addition, a section of the two topography profiles was plotted in Figure 14 for comparison. The root mean square roughness is only 90 pm for the measurement with

the machine table switched off. In contrast, a roughness with the table switched on in closed-loop control was 144 pm.

In general, it can be stated that the influence of the z noise of the setup of the NFM-100 in the range clearly below 1 nm and the AFM measurements are not significantly influenced by the machine table.

In the future, the focus will be on nanofabrication using FESPL. Large-area structures in the form of spirals, circles and lines are to be fabricated and investigated in terms of accuracy and repeatability.

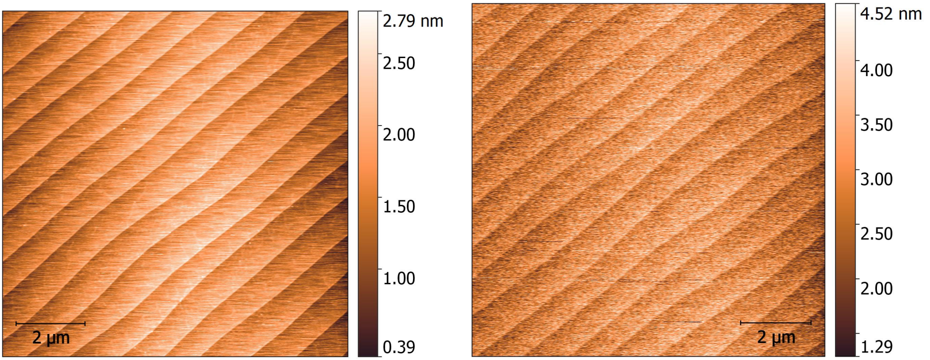

Figure 13. Non-contact AFM images of a 6H-SiC [28] sample with a step height of 0.75 nm with the machine table of the NFM-100 switched off (**left**) and the table switched on in closed-loop control (**right**). The scanning speed for this measurement was 5 µm/s.

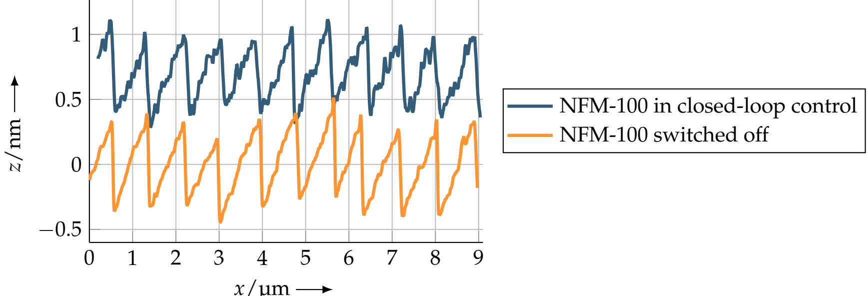

Figure 14. Comparison of the line profiles (taken from AFM images in Figure 13) with the NFM-100 switched on in closed-loop control and switched off.

5. Conclusions and Outlook

The demand for nanostructuring on large areas with the highest possible throughput is constantly increasing. Velocity also plays a major role in how fast as many nanostructures as possible can be produced on wafer sizes. Tip-based technology specifically has its limits in terms of velocity in the millimetre per second range. However, there are some techniques, such as laser-based direct writing and autofocus sensors, that can easily keep up with these velocities. It is of great importance to be able to perform sub-nanometre positioning at high speeds in order to be able to make precise measurements of surface topographies.

This paper presented a newly developed positioning machine and its motion precision in the higher speed range. First, the static condition was considered and then the dynamic positioning properties were examined in more detail. Both linear and circular movements were performed and analysed in relation to the set trajectory. In addition, the maximum movement of the table in the z direction was checked with the existing tip-based system. It was thus possible to find out that the noise of the slider and/or the machine setup is clearly below 1 nm.

Future contributions will focus on nanofabrication. It is indeed already possible to carry out spiral movements, which could be of importance in the future for production by lithography. The ability to easily switch between the measuring mode and the writing mode

of the tip-based system [29–31] will demonstrate patterning with line widths below 100 nm over a large range of motion. Due to the low noise of the stage in all three dimensions, it can be guaranteed that the structuring as well as measurements of the surface are not significantly influenced by the movement of the stage. The comparison of the two AFM images with structure heights of 0.75 nm with the table switched on and off has shown that the noise of the table in the z direction has a minor influence on the AFM measurements. Nevertheless, this can be optimised in the future by additional adaptive control [32] with the use of a third axis [33].

Author Contributions: Conceptualisation, D.D., E.L., S.H., I.R. and E.M.; methodology, J.S. and I.O.; validation, J.S. and J.B.; investigation, J.S.; writing—original draft preparation, J.S.; writing—machine control, J.B., J.S. and S.H.; writing—review and editing, J.S., I.O., J.B. and E.M.; visualisation, J.S.; supervision, E.M. and I.O.; project administration, E.M. and I.O. All authors have read and agreed to the published version of the manuscript.

Funding: This research was funded by the state Thuringia and the European Regional Development Fund (ERDF) in the scope of the program "Promotion of research, technology and innovation", under contract 2018VF0008 and 2018FE9020, and the Deutsche Forschungsgemeinschaft (DFG) in the scope of the program "Forschungsgroßgeräte", under contract INST 273/75-1 FUGG.

Institutional Review Board Statement: Not applicable.

Informed Consent Statement: Not applicable.

Data Availability Statement: Research data are available upon request to the authors.

Acknowledgments: This research was supported by the Deutsche Forschungsgemeinschaft (DFG) in the scope of the Research Training Group "Tip- and laser-based 3D-Nanofabrication in extended macroscopic working areas" (GRK 2182) at Technische Universität Ilmenau. The authors also thank Michael Katzschmann for the fruitful discussions regarding the control of the machine.

Conflicts of Interest: The authors declare no conflict of interest.

References

1. Chen, Y.; Shu, Z.; Zhang, S.; Zeng, P.; Liang, H.; Zheng, M.; Duan, H. Sub-10-nm fabrication: Methods and applications. *Int. J. Extrem. Manuf.* **2021**, *3*, 032002. [CrossRef]
2. Hoefflinger, B. (Ed.) *Chips 2020*; The @Frontiers Collection; Springer: Berlin, Germany, 2012.
3. The International Roadmap for Devices and Systems 2021. IEEE 2021. Executive Summary. Available online: https://irds.ieee.org/editions/2021/executive-summary (accessed on 11 March 2022).
4. Manske, E. Nanopositioning and Nanomeasuring Machine NPMM-200—Sub-nanometre resolution and highest accuracy in extended macroscopic working areas. In Proceedings of the 17th International Conference of the European Society for Precision Engineering and Nanotechnology, Hannover, Germany, 29 May–2 June 2017; pp. 81–82.
5. Ortlepp, I.; Fröhlich, T.; Füßl, R.; Reger, J.; Schäffel, C.; Sinzinger, S.; Strehle, S.; Theska, R.; Zentner, L.; Zöllner, J.P.; et al. Tip- and Laser-based 3D Nanofabrication in Extended Macroscopic Working Areas. *Nanomanuf. Metrol.* **2021**, *4*, 132–148. [CrossRef]
6. Binnig, G.; Quate, C.F.; Gerber, C. Atomic force microscope. *Phys. Rev. Lett.* **1986**, *56*, 930–933. [CrossRef] [PubMed]
7. Michihata, M. Surface-Sensing Principle of Microprobe System for Micro-Scale Coordinate Metrology: A Review. *Metrology* **2022**, *2*, 46–72. [CrossRef]
8. Jäger, G.; Manske, E.; Hausotte, T.; Büchner, H.J. The metrological basis and operation of nanopositioning and nanomeasuring machine NMM-1. *tm-Tech. Mess.* **2009**, *76*, 227–234. [CrossRef]
9. Manske, E.; Fröhlich, T.; Füßl, R.; Ortlepp, I.; Mastylo, R.; Blumröder, U.; Dontsov, D.; Kühnel, M.; Köchert, P. Progress of nanopositioning and nanomeasuring machines for cross-scale measurement with sub-nanometre precision. *Meas. Sci. Technol.* **2020**, *31*, 085005. [CrossRef]
10. Stauffenberg, J.; Reuter, C.; Ortlepp, I.; Holz, M.; Dontsov, D.; Schäffel, C.; Zöllner, J.P.; Rangelow, I.; Strehle, S.; Manske, E. Nanopositioning and -fabrication using the Nano Fabrication Machine with a positioning range up to Ø 100 mm. In Proceedings of the SPIE, Novel Patterning Technologies 2021, Online, 22–27 February 2021; Volume 11610, p. 1161016.
11. Stauffenberg, J.; Ortlepp, I.; Blumröder, U.; Dontsov, D.; Schäffel, C.; Holz, M.; Rangelow, I.W.; Manske, E. Investigations on the positioning accuracy of the Nano Fabrication Machine (NFM-100). *tm-Tech. Mess.* **2021**, *88*, 581–589. [CrossRef]
12. Jäger, G.; Hausotte, T.; Manske, E.; Büchner, H.J.; Mastylo, R.; Dorozhovets, N.; Hofmann, N. Nanomeasuring and nanopositioning engineering. *Measurement* **2010**, *43*, 1099–1105. [CrossRef]
13. Abbe, E. Messapparate für Physiker [Measuring Instruments for Physicists]. *Z. Instrumentenkunde (J. Sci. Instrum.)* **1890**, *10*, 446–448.

14. Hausotte, T. *Nanopositionier- und Nanomessmaschinen—Geräte für die Hochpräzise Makro- bis Nanoskalige Oberflächen- und Koordinatenmessungen Habilitationsschrift*; Technische Universität Ilmenau: Ilmenau, Germany, 2010.
15. Manske, E. Nanofabrication in extended areas on the basis of nanopositioning and nanomeasuring machines. In Proceedings of the SPIE , Novel Patterning Technologies for Semiconductors, MEMS/NEMS, and MOEMS 2019, San Jose, CA, USA, 24–28 February 2019; Volume 10958, p. 109580P.
16. Jäger, G.; Manske, E.; Hausotte, T.; Büchner, H.J. Nano Measuring Machine for Zero Abbe Offset Coordinatemeasuring. *tm-Tech. Mess.* **2000**, *67*, 319. [CrossRef]
17. Ortlepp, I.; Kühnel, M.; Hofmann, M.; Weidenfeller, L.; Kirchner, J.; Supreeti, S.; Mastylo, R.; Holz, M.; Michels, T.; Füßl, R.; et al. Tip- and laser-based nanofabrication up to 100 mm with sub-nanometre precision. In Proceedings of the SPIE, Novel Patterning Technologies for Semiconductors, MEMS/NEMS and MOEMS 2020, San Jose, CA, USA, 23–27 February 2020; Volume 11324, p. 113240A.
18. Manske, E.; Fröhlich, T.; Füssl, R.; Mastylo, R.; Blumröder, U.; Köchert, P.; Birli, O.; Pruss, C.; Schwesinger, F.; Meister, A. Scale spanning subnanometer metrology up to ten decades. In Proceedings of the Optical Measurement Systems for Industrial Inspection XI, Munich, Germany, 24–27 June 2019; pp. 130–136. [CrossRef]
19. Widdershoven, I.; Donker, R.L.; Spaan, H.A.M. Realization and calibration of the "Isara 400" ultra-precision CMM *J. Phys. Conf. Ser.* **2020**, *311*, 012002. [CrossRef]
20. Ortlepp, I.; Stauffenberg, J.; Manske, E. Processing and Analysis of Long-Range Scans with an Atomic Force Microscope (AFM) in Combination with Nanopositioning and Nanomeasuring Technology for Defect Detection and Quality Control *Sensors* **2021**, *21*, 5862. [CrossRef] [PubMed]
21. New Way Air Bearings. Advantages of Air Bearings. Available online: https://newwayairbearings.com/technology/design-basics/advantages-of-air-bearings/ (accessed on 28 June 2022).
22. Differenz-Interferometer SP 5000 DI. Data Sheet. SIOS Meßtechnik GmbH. 2022. Available online: https://www.sios-precision.com/fileadmin/user_upload/Produkte/Produktdetails/Flyer/differenz-interferometer_SP_DI_dt_flyer.pdf (accessed on 8 July 2022).
23. Hesse, S.; Schäffel, C.; Mohr, H.U.; Katzschmann, M.; Büchner, H.J. Design and performance evaluation of an interferometric controlled planar nanopositioning system. *Meas. Sci. Technol.* **2012**, *23*, 074011. [CrossRef]
24. Zschäck, S.; Hesse, S.; Amthor, A.; Katzschmann, M.; Schäffel, C.; Ament, C. Vergleich der Scan-Performance bei Nanopositioniersystemen mit großem Bewegungsbereich *tm-Tech. Mess.* **2014**, *81*, 335–342. [CrossRef]
25. Differenz-Interferometer SP 5000 DI. Technical Data. SIOS Meßtechnik GmbH. 2022. Available online: https://www.sios-precision.com/fileadmin/user_upload/Produkte/Produktdetails/Datenblaetter/datenblatt-laser-interferometer-SP-DI-dt.pdf (accessed on 15 June 2022).
26. *Nanofabrikationsmaschine 100—SP-NanoFab100*; Technical Data; SIOS Meßtechnik GmbH: Ilmenau, Germany, 2022.
27. Grimble, M.J. *Robust Industrial Control: Optimal Design Approach for Polynomial Systems*; Prentice Hall: Hoboken, NJ, USA, 1994; pp. 261, 443–456. ISBN 978-0-470-02073-9.
28. NT-MDT Spectrum Instruments Product SiC/0.75. 2022. Available online: https://www.ntmdt-tips.com/products/view/sic-0-75 (accessed on 8 March 2022).
29. Rangelow, I.W.; Ivanov, T.; Hudek, T.; Fortagne, O. Device and Method for Mask-Less AFM Microlithography. U.S. Patent US7141808B2, 13 October 2005.
30. Nano Analytik GmbH. SEM Image Microcantilever. 2020. Available online: https://www.nanoanalytik.net/products/probes/afm-canti/ (accessed on 1 August 2021).
31. Kaestner, M.; Rangelow, I.W. Scanning probe lithography on calixarene towards single-digit nanometer fabrication. *Int. J. Extrem. Manuf.* **2020**, *2*, 032005. [CrossRef]
32. Shao, K.; Zheng, J.; Tang, R.; Li, X.; Man, Z.; Liang, B. Barrier Function Based Adaptive Sliding Mode Control for Uncertain Systems With Input Saturation. *IEEE/ASME Trans. Mechatron.* **2022**. [CrossRef]
33. Gorges, S.; Hesse, S.; Schäffel, C.; Ortlepp, I.; Manske, E.; Langlotz, E.; Dontsov, D. Integrated Planar 6-DOF Nanopositioning System. *IFAC-PapersOnLine* **2019**, *52*, 313–318. [CrossRef]